

Homogeneous cooling of rough, dissipative particles: Theory and simulations

S. Luding⁽¹⁾, M. Huthmann⁽²⁾, S. McNamara^(1;3), A. Zippelius⁽²⁾

(1) Institute for Computer Applications 1, Pfaffenwaldring 27, 70569 Stuttgart, GERMANY

(2) Institut für Theoretische Physik, Universität Göttingen, Bunsenstr. 9, 37073 Göttingen, GERMANY

(3) Levich Institute, Steinman Hall T-1M, 140th St and Convent Ave, New York, NY 10031, USA

(December 28, 2021)

We investigate freely cooling systems of rough spheres in two and three dimensions. Simulations using an event driven algorithm are compared with results of an approximate kinetic theory, based on the assumption of a generalized homogeneous cooling state. For short times, translational and rotational energy are found to change linearly with t . For large times both energies decay like t^{-2} with a ratio independent of time, but not corresponding to equipartition. Good agreement is found between theory and simulations, as long as no clustering instability is observed. System parameters, i.e. density, particle size, and particle mass can be absorbed in a rescaled time, so that the decay of translational and rotational energy is solely determined by normal restitution and surface roughness.

PACS: 51.10.+y, 46.10.+z, 05.60.+w, 05.40.+j

I. INTRODUCTION

Collections of microscopic, dissipative, and rough constituents have attracted a lot of interest recently, mainly in the context of granular media [1,3]. In the so-called grain-inertia regime, one is concerned with rapid granular flow, which on one hand can be described by methods of statistical mechanics, analogous to the kinetic theory of dense gases [4,8], and, on the other hand, can be well simulated with help of event-driven algorithms [9,10]. In both approaches the dynamics of the system is assumed to be dominated by two-particle collisions which are modelled by their asymptotic states. A collision is characterized by the velocities before and after the contact, and the contact is assumed to be instantaneous. In the simplest model, one describes inelastic collisions by normal restitution only. However, surface roughness is important for the dynamics of granular flow [8,10] and allows for an exchange of translational and rotational energy.

The rough sphere model was first introduced for elastically colliding particles, assuming either perfectly rough or perfectly smooth particles [11,12]. Subsequently, it has been generalised to intermediate values of the roughness to account for tangential restitution in inelastic collisions. Several groups have investigated the exchange of translational and rotational energy, using kinetic theory [4,8] or numerical simulations [9,10]. One major result is that in contrast to conservative systems, energy is not equipartitioned between the degrees of freedom in dissi-

pative systems [4,10], even though the ratio of translational and rotational energy approaches a constant, while both functions decay to zero in a freely cooling system. In this paper we study the full time evolution of translational and rotational energy of a gas of rough, hard spheres. We compare numerical simulations to kinetic theory, which is based on a pseudo-Liouville operator formalism and makes use of the assumption of a homogeneous state. The computation covers the full range of times, from the initial linear change of energies with time, to the asymptotic state for large times, and also including the crossover between the two limiting regimes.

In section II we introduce the microscopic interaction laws and the operators needed in section III to derive the solution for homogeneously cooling systems. The analytical solution is compared to the simulations in section IV and the results are summarized and discussed in V.

II. MICROSCOPIC DYNAMICS

We consider a system of N D -dimensional spheres interacting via a hard-core potential confined to a D -dimensional volume $V = L^D$ with linear size L and $D = 2$ or 3 . The spheres have mass m , radius a , and moment of inertia I . The degrees of freedom are the positions $\mathbf{r}(t)$, the translational velocities $\mathbf{v}(t)$, and the angular velocities $\boldsymbol{\omega}(t)$ for each sphere, numbered by $i = 1; 2; \dots; N$. Here, the spheres are rough with constant normal and also constant tangential restitution. The translational and angular velocities after collision (primed quantities) are determined by the velocities before collision (unprimed quantities) so that

$$\mathbf{v}' = \mathbf{v} - \frac{1+r}{2} v_n \frac{\mathbf{q}(1+\epsilon)}{2q+2} (\mathbf{v}_t + \mathbf{v}_r); \quad (1)$$

$$\mathbf{v}' = \mathbf{v} + \frac{1+r}{2} v_n + \frac{\mathbf{q}(1+\epsilon)}{2q+2} (\mathbf{v}_t + \mathbf{v}_r); \quad (2)$$

$$\boldsymbol{\omega}' = \boldsymbol{\omega} + \frac{1+\epsilon}{a(2q+2)} [\hat{\mathbf{r}} \times (\mathbf{v}_t + \mathbf{v}_r)]; \text{ and} \quad (3)$$

$$\boldsymbol{\omega}' = \boldsymbol{\omega} + \frac{1+\epsilon}{a(2q+2)} [\hat{\mathbf{r}} \times (\mathbf{v}_t + \mathbf{v}_r)]; \quad (4)$$

The unit vector $\hat{\mathbf{r}} = (\mathbf{r}_i - \mathbf{r}_j) = r_j - r_i$ points from particle i to j , along the line connecting the centres of mass. We have introduced abbreviations for the normal

velocity $v_n = [(v \quad v) \hat{r}] \hat{r}$, for the tangential velocity due to translational motion $v_t = v - v \hat{r}$ and for the tangential velocity due to rotational motion $v_r = a(\hat{r} \times \hat{r}) \hat{r}$. The constants r and q characterize normal and tangential restitution, and $q = I/(m a^2)$ depends on the mass distribution inside a grain.

The time evolution of a dynamical variable $A(t) = A(\mathbf{r}; \mathbf{v}; \mathbf{l}; t)$ is (for positive times) determined by the pseudo-Liouville operator L_+

$$A(t) = \exp(iL_+ t) A(0) \quad (5)$$

The pseudo-Liouville operator [8,13,14] consists of two parts $L_+ = L_0 + L_+^0$. The first, L_0 , describes the undisturbed motion of single particles

$$L_0 = \sum_i \mathbf{v}_i \cdot \nabla_{\mathbf{r}_i} + \sum_i \mathbf{l}_i \cdot \nabla_{\mathbf{l}_i} \quad (6)$$

and the second, $L_+^0 = \frac{1}{2} \sum_{i,j} C_{ij}(\mathbf{r}_i, \mathbf{r}_j)$, describes hard-core collisions of all pairs of particles (i, j) with

$$C_{ij}(\mathbf{r}) = i(\mathbf{v}_i \cdot \hat{r}) (\mathbf{v}_j \cdot \hat{r}) (\mathbf{r}_i - \mathbf{r}_j - 2a) \delta^3(\mathbf{r} - \mathbf{r}_{ij}) \quad (7)$$

The operator b^+ acts on the particles i and j only, and instantaneously replaces the translational and angular momenta just before the collision, by the corresponding values just after. $(\mathbf{v}_i \cdot \hat{r})$ is the Heaviside step function which is non-zero for approaching particles only. The term $\mathbf{v}_i \cdot \hat{r}$ gives the relative velocity of two colliding particles, reflecting that fast particles collide more frequently. Finally, we have introduced the notation $\mathbf{v} = \mathbf{v}_i - \mathbf{v}_j$, $\mathbf{r} = \mathbf{r}_i - \mathbf{r}_j$, and $\hat{r} = \mathbf{r}/r$.

III. HOMOGENEOUS COOLING STATE

The ensemble average of a dynamical variable $A(\mathbf{r}; \mathbf{v}; \mathbf{l}; t)$ is defined by

$$\langle A \rangle_t = \int d\mathbf{r} d\mathbf{v} d\mathbf{l} (\mathbf{r}; \mathbf{v}; \mathbf{l}; t) A(\mathbf{r}; \mathbf{v}; \mathbf{l}; 0) \quad (8)$$

with the abbreviation for phase space integration

$$\int d = \int d\mathbf{r} d\mathbf{v} d\mathbf{l} \delta^3(\mathbf{r} - \mathbf{r}_{ij} - 2a) \quad (9)$$

Here $(\mathbf{r}; \mathbf{v}; \mathbf{l}; t)$ is the N -particle phase space distribution function, i.e. $(\mathbf{r}; \mathbf{v}; \mathbf{l}; t) d$ is the probability at time t to find particle 1 at $(\mathbf{r}_1; \mathbf{v}_1; \mathbf{l}_1)$, particle 2 at $(\mathbf{r}_2; \mathbf{v}_2; \mathbf{l}_2)$, etc. The time evolution of the N -particle distribution $(\mathbf{r}; \mathbf{v}; \mathbf{l}; t) = \exp(-iL_+^0 t) (\mathbf{r}; \mathbf{v}; \mathbf{l}; 0)$ is governed by the adjoint L_+^0 of the time evolution operator L_+ .

The quantities of interest are the translational and rotational energies per particle $E_{tr} = m(2N)^{-1} \sum_i v_i^2$ and

$E_{rot} = I(2N)^{-1} \sum_i l_i^2$, as well as the total kinetic energy $E = E_{tr} + E_{rot}$. It is in principle possible to calculate these expectation values exactly. To make some progress we resort to an approximation, known as homogeneous cooling state. One assumes that the N -particle distribution function is spatially homogeneous and depends on time only via the average kinetic energy of the grains. It was shown in [8] that initially equipartitioned translational and rotational energy change with different rates, suggesting a generalised cooling state of the form

$$h_{CS}(\mathbf{r}; \mathbf{v}; \mathbf{l}; t) = \exp\left[-N \left(\frac{E_{tr}}{T_{tr}(t)} + \frac{E_{rot}}{T_{rot}(t)} \right) \right] \quad (10)$$

The N -particle distribution does not depend on the spatial coordinates \mathbf{r} as a consequence of the assumption of homogeneity. It depends on time only via the average translational and rotational energy: $T_{tr}(t) = 2D \langle E_{tr} \rangle_t$ and $T_{rot}(t) = 2(2D-3) \langle E_{rot} \rangle_t$. The factors D and $2D-3$ account for the number of translational and rotational degrees of freedom in D dimensions respectively. To study the time evolution of the average translational and rotational energy we consider the corresponding time derivatives:

$$\begin{aligned} \frac{d}{dt} T_{tr}(t) &= \frac{2}{D} \int d(\mathbf{r}; \mathbf{v}; \mathbf{l}; t) iL_+ E_{tr} \quad \text{and} \\ \frac{d}{dt} T_{rot}(t) &= \frac{2}{2D-3} \int d(\mathbf{r}; \mathbf{v}; \mathbf{l}; t) iL_+ E_{rot} \quad (11) \end{aligned}$$

Then, we assume the generalized homogeneous cooling state of Eq. (10), replacing $(\mathbf{r}; \mathbf{v}; \mathbf{l}; t)$ by $h_{CS}(\mathbf{r}; \mathbf{v}; \mathbf{l}; t)$ in Eqs. (11), and arrive at

$$\begin{aligned} \frac{d}{dt} T_{tr}(t) &= \frac{2}{D} \langle iL_+ E_{tr} \rangle_{h_{CS}} \quad \text{and} \\ \frac{d}{dt} T_{rot}(t) &= \frac{2}{2D-3} \langle iL_+ E_{rot} \rangle_{h_{CS}} \quad (12) \end{aligned}$$

All that remains to be done is a high dimensional phase space integral, the details of which are delegated to appendix A, where we present calculations for $D=2$. After integration over phase space has been performed, we find

$$\begin{aligned} \langle iL_+ E_{tr} \rangle_{h_{CS}} &= GA T_{tr}^{3=2} + GB T_{tr}^{1=2} T_{rot} \quad \text{and} \\ \langle iL_+ E_{rot} \rangle_{h_{CS}} &= GB T_{tr}^{3=2} - GC T_{tr}^{1=2} T_{rot} \quad (13) \end{aligned}$$

with the constants A, B, C , and G , whose values depend on space dimensionality D .

A. The 2D-C case

In two dimensions the constants in Eqs. (13) are given by

$$\begin{aligned} G &= 8a \frac{N}{V} \frac{r}{m} g(2a); & A &= \frac{1}{4} \frac{r^2}{a^2} + \frac{1}{2} (1 - q); \\ B &= \frac{2}{2q}; & C &= \frac{1}{2q} - \frac{1}{q} \quad (14) \end{aligned}$$

We have introduced the abbreviation $\beta = q(1 + \mu) = (2q + 2)$, and $g(2a)$ denotes the pair correlation function at contact. We consider homogeneous discs with $q = 1 = 2$.

In a system of elastically colliding particles [12], $G T_{tr}^{1=2}$ is just the Enskog collision frequency, whose inverse determines the mean time between collisions. We use this mean collision frequency of the elastic system to rescale time according to $t = G T_{tr}^{1=2}(0) t$, and furthermore introduce the dimensionless translational temperature $T = T_{tr}(t) = T_{tr}(0)$ and the dimensionless rotational temperature $R = T_{rot}(t) = T_{tr}(0)$. Expressed in scaled units Eqs. (12) and (13) read in 2D :

$$\begin{aligned} \frac{d}{dt} T &= -A T^{3=2} + B T^{1=2} R; \\ \frac{d}{dt} R &= 2B T^{3=2} - 2C T^{1=2} R; \end{aligned} \quad (15)$$

To find the asymptotic value of the ratio of $K = T/R$ we consider the differential equation

$$\frac{dT}{dR} = \frac{AK + B}{2BK - 2C}; \quad (16)$$

which can be solved by a constant

$$K = \frac{2C}{A} + \frac{B}{(2C/A)^2 + 8B^2} = (4B) \quad (17)$$

in agreement with Ref. [10].

Of particular interest is the long time decay of translational and rotational energy as a function of r and μ . We would expect the decay to be slowest, if energy is lost only due to normal restitution and not due to roughness. Hence, as a function of μ , translational and rotational energy should persist for the longest times for $\mu = 1$. In between, i.e. $1 < \mu < 1$, we expect a faster decay, because surface roughness is an additional mechanism for the dissipation of energy. These expectations are born out by the following detailed discussion of Eqs.(15,17). We assume that the ratio $K = T/R$ has reached its asymptotic value given in Eq. (17) for some $t > 0$ and substitute $R = T/K$ into Eq. (15) and obtain

$$\frac{d}{dt} T = -F T^{3=2}; \quad (18)$$

The resulting equation is of the same functional form as for homogeneous cooling of smooth spheres, except for the coefficient $F = A - B/K$, which contains all the dependence on μ and r . Its solution is given by

$$T = \frac{T(0)}{1 + T(0)^{1=2} (F=2) (t(0))^2}; \quad (19)$$

Asymptotically, for $\mu \rightarrow 1$, the translational energy decays like $T \propto (t(0))^{-2}$ and the rotational energy like $R \propto (t(0))^{-2}$. In a double-logarithmic plot of T and

R against t one should observe straight lines with slope -2 and axial sections (at $t = 1$) given by $\ln T(0)$ ($F=2$) for the translational energy, and by $\ln(F/K=2)$ for the rotational energy. For the same slope a larger axial section implies persistence for longer times, i.e. a 'slower' decay in time. In Fig. 1 we plot the prefactors F and F/K against β for $r = 0.99$.

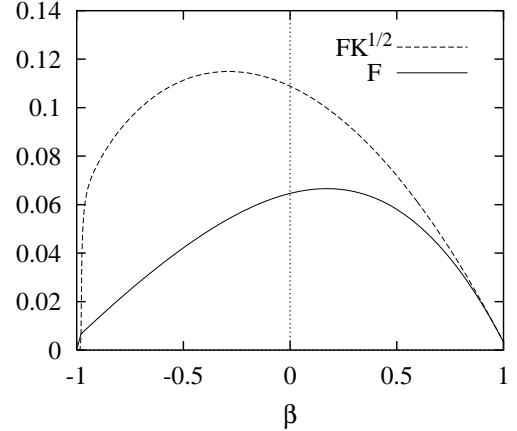


FIG. 1. Dependence of the asymptotic decay-prefactors F and F/K on β for $r = 0.99$.

As a function of μ , F is smallest for $\mu = 1$ corresponding to the cases where no energy is lost due to friction. The decay of translational energy is then pushed out to the longest timescales. In Fig. 1, the maximum of F is reached for $\mu_{tr}^{max} = 0.17$, corresponding to the 'fastest' decay of T . For $\mu = 1$ we find that $F/K = 0$, because the rotational energy remains constant as a function of time. F/K reaches its maximum for $\mu_{rot}^{max} = 0.29 \in \mu_{tr}^{max}$, so that the decay of rotational energy is 'fastest' for a value of μ , different from the one where the translational energy decays fastest. In the limit $\mu \rightarrow 1$ the axial sections for T and R have approximately the same values. In this case the ratio K is close to unity, reflecting the rather effective exchange of rotational and translational energy for rough spheres and thus approximate equipartition.

B. The 3D -Case

In 3D we consider spheres with $q = 2 = 5$. The constants in Eq. (13) are given by

$$\begin{aligned} G &= 8(2a)^2 \frac{N}{V} \frac{r}{m} g(2a); & A &= \frac{1}{4} \frac{r^2}{4} + (1 - \mu); \\ B &= \frac{2}{q}; & C &= \frac{1}{q} - \frac{1}{q} \mu; \end{aligned} \quad (20)$$

As in two dimensions we introduce a dimensionless time $t = \frac{2}{3} G T_{tr}^{1=2}(0) t$ with the factor $2=D = 2=3$, which ac-

counts for the number of translational degrees of freedom. The time dependence of the dimensionless translational temperature $T = T_{tr}(t) = T_{tr}(0)$ and of the dimensionless rotational temperature $R = T_{rot}(t) = T_{tr}(0)$ follows from

$$\begin{aligned} \frac{d}{dt}T &= -AT^{3/2} + BT^{1/2}R; \\ \frac{d}{dt}R &= -BT^{3/2} - CR^{1/2}R; \end{aligned} \quad (21)$$

The asymptotic value of the ratio of $K = T/R$ is given in Refs. [7] and [10]:

$$K = C \frac{A}{A + \frac{C}{4B^2}} = (2B) : \quad (22)$$

The long time limit can be discussed as in the 2D case. We find a very similar result for the dependence of the asymptotic decay on r and ϵ .

The full time dependent solution, obtained by numerical integration of Eqs. (15) and (21), will be compared with simulations in the next section.

IV. NUMERICAL EXPERIMENTS

Since we are interested in the behavior of granular particles cooling over several decades in time, we use an event driven (ED) method. In these simulations, the particles follow an undisturbed translational motion until an event occurs. An event is either the collision of two particles or the collision of one particle with a boundary of a cell (in the linked-cell structure). The cells have no effect on the particle motion here; they were solely introduced to accelerate the search for future collision partners in the algorithm (see also Appendix B). Using the velocities just before contact we compute the particles' velocities just after the contact following Eqs. (1-4). In the ED method the contact duration is implicitly zero, matching well the corresponding assumption of instantaneous contacts used for the theory. We remark that ED algorithms run into problems when the time between events t_{ev} gets too small. In dense systems with strong dissipation t_{ev} may tend towards zero. As a consequence the so-called "inelastic collapse" can occur, i.e. the divergence of the number of events per unit time. The problem of the inelastic collapse [15,16], can be handled using restitution coefficients dependent on the time elapsed since the last event [17,18]. For the contact that occurs at time t_{ij} , one uses $r = 1$ and $\epsilon = 1$ if at least one of the involved partners had a collision with another particle later than $t_{ij} - t_c$. The time t_c can be identified as a typical duration of a contact. The effect of t_c on the simulation results is negligible for large r and small t_c , what we checked in the simulations. Only for very small values $r \approx 0.6$ a cut-off time $t_c = 10^{-6}$ s was needed to avoid the inelastic collapse. For a more detailed discussion of the ED algorithm used, see Appendix B.

Every simulation is first equilibrated with $r = 1$ and $\epsilon = 1$ until the velocity distribution is Maxwellian. Then the restitution coefficients are set to the selected values. In order to classify the systems used for the simulations we need to specify the number of particles N and the volume fractions $\phi_{2D} = (N/V) a^2$ and $\phi_{3D} = (N/V) (4/3) a^3$ in two and three dimensions, respectively.

A. Results in 2D

For short times we can solve Eqs. (15) analytically and get $T = 1 - A$ and $R = (2B)A$. Hence our data can be effectively collapsed for short times by rescaling time according to \sqrt{A} and rotational temperature according to $R/\sqrt{A} = (2B)$. We compare the theoretical result [numerical solution of Eq. (15)] with simulations for various sets of parameters. The scaling collapses data for different particle number, particle radius and density on the same master curves, since all these dependencies are hidden in the rescaled time. The shape of the master curves depends only on the restitution coefficients r and ϵ . In order to check the dependence of the solution on system size we simulate a large system with $N = 99856$ particles and a small system with only $N = 198$. For the small system we consider two volume fractions $\phi = 0.25$ or $\phi = 0.01$, the latter corresponding to an extremely dilute system. For the large system we always use $\phi = 0.25$. For the larger volume fraction we get numerically $g_{0.25}(2a) = 1.58$ in perfect agreement with the 2D equivalent of the Camahan-Stirling formula

$$g(2a) = \frac{1}{(1 - \frac{7}{16})^2}; \quad (23)$$

from Ref. [19]. Initially, the normalized energies are $T = 1$ and $R = 0$ for all data presented here.

In Fig. 2 we plot T against rescaled time \sqrt{A} for various simulations with fixed value of $r = 0.99$ and different particle number N , volume fraction ϕ , and tangential restitution ϵ . We observe that all simulations with the same ϵ collapse, independent of the specific value of N or ϕ . This indicates that the dimensionless units T and R are indeed the system's inherent "temperature" and "time". The temperature T decays continuously from its initial value $T = 1$, following the function $T = 1 - A$ for short times $\sqrt{A} < 0.1$ and decaying like A^{-2} for long times. The monotonic dependence of T on \sqrt{A} is due to our scaling of the horizontal axis, which includes factors of \sqrt{A} . If we plot T against A we observe that the crossover between the initial linear decay and the asymptotic A^{-2} behavior is nonmonotonic with ϵ : The time of crossover is largest for $\epsilon = 1$, then decreases and reaches a minimum around $\epsilon_{tr}^{max} \approx 0.17$ and then increases again for $\epsilon > 1$ [in agreement with Fig. 1].

The simulations of the large system deviate from the theory and also from the simulations for the small system

at large times or small T . The deviation from the theoretical curve is due to the density instability, i.e. clusters of particles form and the homogeneous cooling assumption fails. Additional simulations show that the deviation from theory occurs earlier for stronger dissipation due to either smaller r or j .

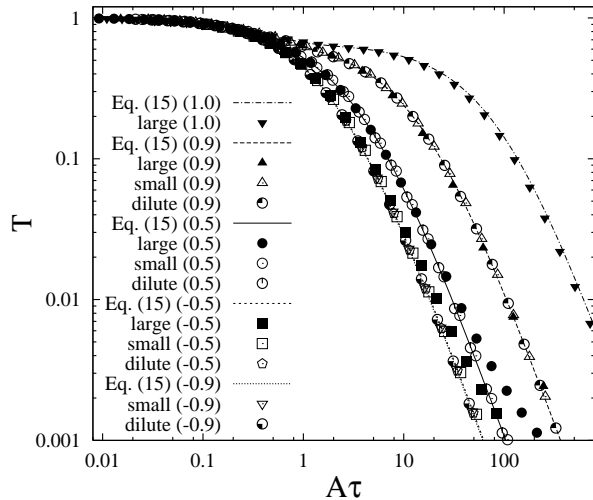


FIG. 2. T as function of rescaled time $A\tau$. Different symbols correspond to different simulations with $N = 99856$, $\rho = 0.25$ (large), $N = 198$, $\rho = 0.25$ (small), and $N = 198$, $\rho = 0.01$ (dilute). The coefficient of restitution is $r = 0.99$ and the value of j is given in brackets in the inset. The curves represent numerical solutions of Eqs. (15).

In Fig. 3 we plot $RA = \langle 2B \rangle$ against normalized time $A\tau$ for the same set of parameters as in Fig. 2. As expected from the solution for small $A\tau$, we find that $RA = \langle 2B \rangle$ is proportional to $A\tau$ for small times $A\tau < 0.1$. In this regime, the initially 'cold' rotational degrees of freedom are activated due to the transfer of linear to angular momentum during collisions. After some equilibrium between translational and rotational temperature is achieved, both degrees of freedom lose energy in the long time limit. Like the translational temperature, also the rotational temperature is independent of N and ρ , only r and j determine the decay of rotational energy. As for the translational energy, the observed, almost monotonic dependence of the crossover time for the rotational energy on j is due to our scaled units $\tau = A\tau$ and $R = RA = \langle 2B \rangle$. If we plot R against τ we find a similar nonmonotonic dependence of the crossover time on j as for the translational energy with however the minimum of rotational crossover time occurring at a different value of $\tau_{rot}^{max} \approx 0.29$ [see Fig. 1].

The results of simulations are in very good agreement with the theoretical results, which are based on the generalized homogeneous cooling assumption for the N -particle distribution function. Note that the agreement extends over many orders of magnitude in time

and covers the initial increase of R , the crossover and the algebraic decay for long times.

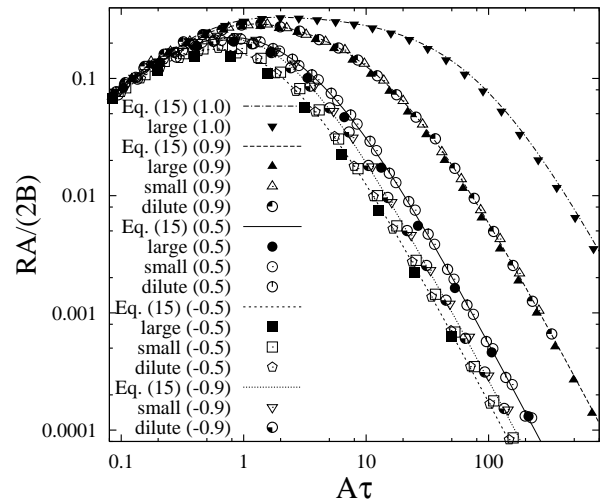


FIG. 3. $RA = \langle 2B \rangle$ as function of rescaled time $A\tau$. The simulations are the same as in Fig. 2. The curves represent the numerical solutions of Eqs. (15).

In Fig. 4 we present the ratio of T and $RA = \langle 2B \rangle$ as a function of scaled time $A\tau$ for a selected set of parameters which were used in the simulations shown in Fig. 2. Data for two values $\rho = 1.0$ and $\rho = 0.5$ are shown in Fig. 4 (a). For the latter we compare systems at different densities and observe that the dilute simulations are in perfect agreement with the theory, whereas the dense system with $\rho = 0.25$ deviates. The small system shows a slightly smaller ratio $(2B = A) T = R$, whereas for the large system, the ratio $(2B = A) T = R$ is larger than expected and eventually diverges for large $A\tau$. This is again the regime where the homogeneous cooling assumption fails. Interestingly, the large simulation with $N = 99856$, $\rho = 0.25$, and $\rho = 1.0$ is in reasonable agreement with theory. From Fig. 4 (b), we learn that the simulations of dilute systems are always in good agreement with theory. The ratio $(2B = A) T = R$ is constant for large times, but there is no equipartition of energies in the translational and rotational degrees of freedom.

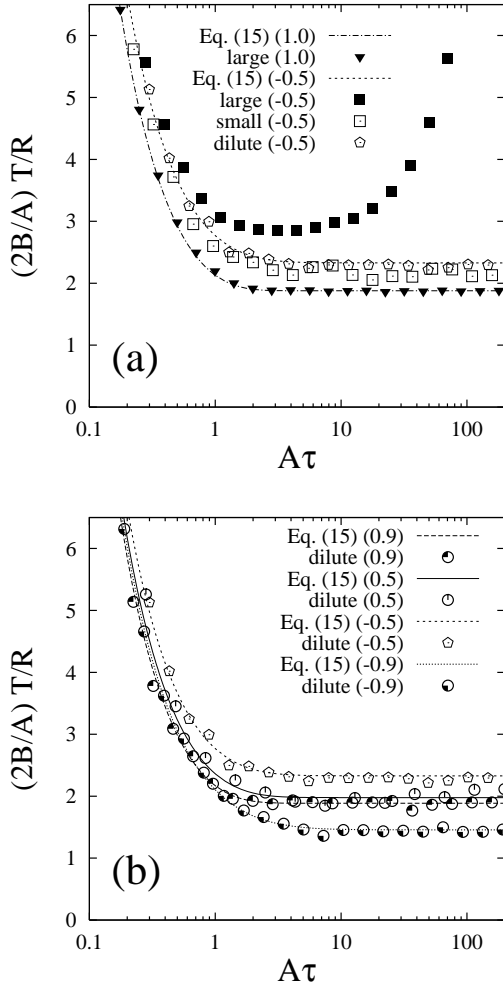


FIG. 4. $(2B/A)T/R$ as a function of rescaled time $A\tau$ for some simulations from Fig. 2. (a) The simulation of the large system with $N = 99856$, $\eta = 0.25$, and $\epsilon = 0.5$ (solid squares) shows no saturation of $(2B/A)T/R$ which instead diverges for large $A\tau$. (b) Here only simulations of the dilute system with $N = 198$, and $\eta = 0.01$ are compared to theory. All show saturation of the ratio $(2B/A)T/R$ for large times.

B. R results in 3D

As in 2D, we can solve Eq. (21) analytically for short times, and get $T = 1 - A$ and $R = B$. Hence we rescale time $\tau \rightarrow A\tau$ and rotational temperature $R \rightarrow RA = B$.

We simulated various systems characterized by volume fraction η and particle number N . One system with density $\eta = 0.087$ and $N = 1331$ particles is denoted as medium; two other systems with lower density have the parameters $\eta = 0.0021$, $N = 4096$ dilute, and $\eta = 0.0023$, $N = 68921$ large. The abbreviation corresponds to the density, only for the large system one should read "dilute and large". Finally, a system with higher density,

ie. $\eta = 0.23$ and $N = 54872$ dense is examined. To calculate the pair correlation function at contact, we use the Camahan-Starling formula

$$4g(2a) = \frac{1 + \frac{2}{3} + \frac{2^2}{3^2} + \frac{2^3}{3^3}}{(1 - \frac{2}{3})^3} \quad 1 = 4 \frac{1 - \frac{2}{3}}{(1 - \frac{2}{3})^3}; \quad (24)$$

in 3D from Ref. [23]. Initially, the normalized energies are $T = 1$ and $R = 0$ for all data presented here.

Constant $r = 0.99$, variable ϵ and

In Fig. 5 we plot T against normalized time $A\tau$ for $r = 0.99$ and various values of the tangential restitution ϵ . We observe a very similar picture as in 2D and, again, reasonable agreement between theory and simulation over many orders of magnitude in time. For $\epsilon < 0.5$ most of the dependence on η is taken into account by our scaling, $\tau \rightarrow A\tau$, so that the scaled data almost collapse for $\epsilon < 0.5$.

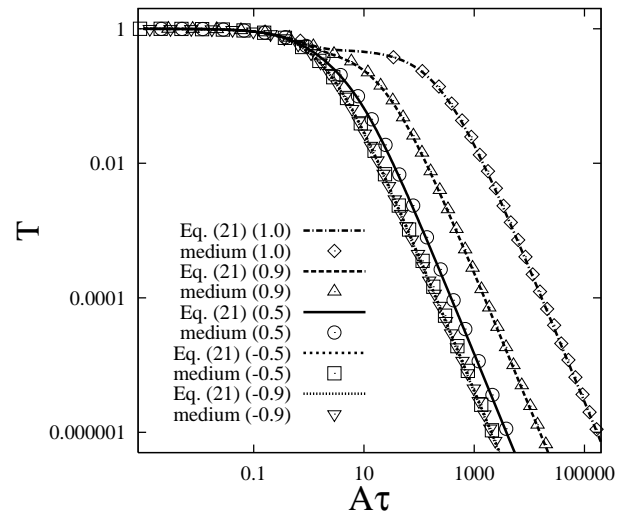


FIG. 5. T as function of rescaled time $A\tau$ in 3D. The symbols correspond to simulations with $N = 1331$, $\eta = 0.087$ (medium), $r = 0.99$, and different ϵ as given in brackets in the inset. The curves represent numerical solutions of Eqs. (21) with the three-dimensional constants from Eqs. (20).

In Fig. 6 we compare simulations of different systems with the numerical solution of Eqs. 21. Only the dense simulations deviate from the theoretical result. The scaling of time with A is rather successful for small and moderately dilute systems; in dense systems a deviation from the theory occurs for large $A\tau$.

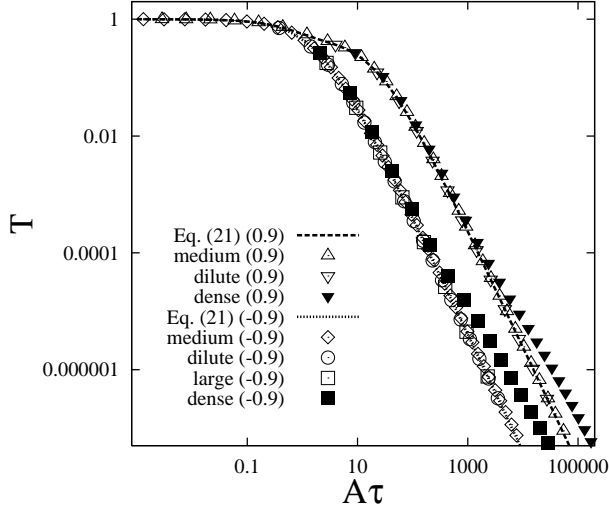


FIG. 6. T as function of rescaled time $A\tau$ in 3D from simulations with $r = 0.99$, and $\epsilon = 0.9$ or $\epsilon = +0.9$ as given in brackets. Different symbols correspond to simulations with $N = 1331$, $\epsilon = 0.087$ (medium), $N = 4096$, $\epsilon = 0.0021$ (dilute), $N = 68921$, $\epsilon = 0.0023$ (large), and $N = 54872$, $\epsilon = 0.23$ (dense). The curves are numerical solutions of Eqs. (21) with the three-dimensional constants from Eqs. (20).

In Fig. 7 we plot $RA=B$ versus normalized time $A\tau$ for medium and dense systems. As in 2D, we find that $RA=B$ increases proportional to A for small times ($A < 0.1$), reflecting the activation of initially 'cold' rotational degrees of freedom due to collisions. This feature as well as the full time dependence is well reproduced by our theoretical analysis.

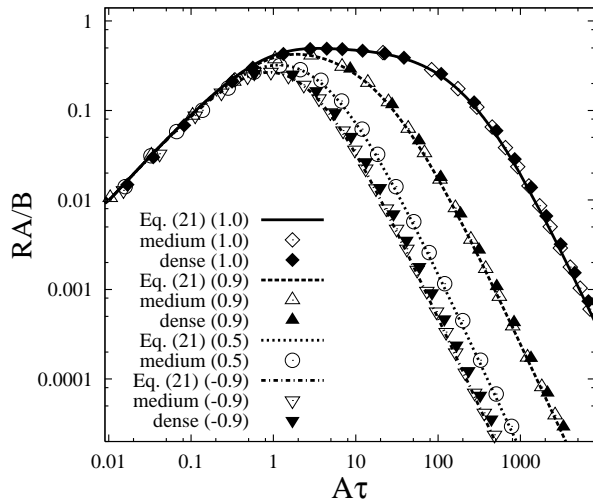


FIG. 7. $RA=B$ as function of rescaled time $A\tau$. The data are selected situations from Fig. 5. The curves represent the numerical solutions of Eqs. (21).

In Fig. 8 we present T , $RA=B$ and the ratio of T and $RA=B$ as a function of scaled time $A\tau$ for $r = 0.6$ and $\epsilon = 0.9$, where interesting structure is observed. The open symbols correspond to the medium system with $\epsilon = 0.087$, $N = 1331$. The data are in good agreement with the theoretical curves, whilst we obtain substantial differences between theory and simulation in the case of the dense system, due to the density instability [not shown here]. For the medium system the loss of energy during collisions is predominantly due to normal restitution and only after the translational energy has decayed to a very small value ($T < 10^{-5}$) does one observe the energy loss due to friction. The two regimes can be discussed analytically with help of Eqs. (21). For intermediate times, when the translational energy is still appreciable, the equations can be simplified for almost smooth spheres, i.e. ($\epsilon = 1$):

$$\frac{d}{d}T = -AT^{3/2} \quad (25)$$

$$\frac{d}{d}R = -CT^{1/2}R : \quad (26)$$

We have neglected terms of $O((1+\epsilon)^2)$ and approximate $A(1-\epsilon^2) = 4$ and $C = 5(1+\epsilon) = 14$. The solution for T is that of smooth spheres, decaying like $T(\tau) \propto (A\tau)^{-2}$ for large τ . Substituting this result into the equation for R , we find $R(\tau) = R_0 + (\epsilon = 0)$ with $\epsilon = 2C\tau = A$. Here τ_0 is some intermediate timescale, larger than the time for the initial increase of R , but smaller than the timescale to reach the true asymptotic state. The above algebraic decay is shown in Fig. 8 as a straight dashed line with slope -0.396 . Once the translational energy has decayed to a very small value as compared to the rotational energy, all terms in the differential equations for R and T are equally important. We then observe a crossover from a τ^{-2} to a τ^{-2} decay of the rotational energy. This true asymptotic state is characterized by a constant ratio $T=R$ and has been discussed above. The crossover between the two regimes shows up as a parallel shift for T [see Figs. 8 and 9], because the translational energy decays like τ^{-2} in both regimes, but with a different prefactor.

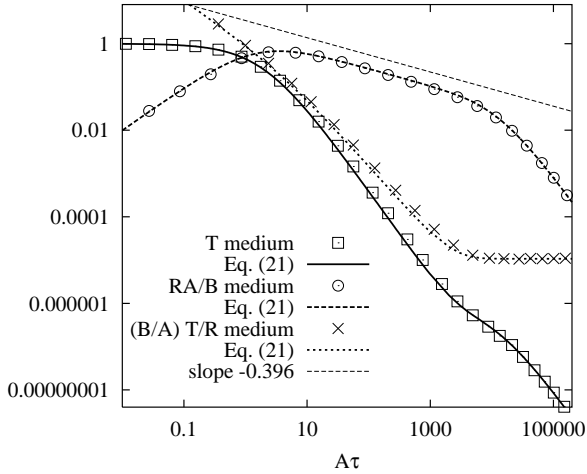


FIG. 8. T , $RA=B$, and $(B=A)T=R$ for 3D simulations with $\rho = 0.9$ and $r = 0.6$ in the medium (open symbols) and in the dense (solid symbols) system from Fig. 5. The thick lines give the solution of Eqs. (21).

When r is increased to a value close to unity, i.e. the elastic case, the intermediate time regime disappears, because normal and tangential restitution are equally important. This is demonstrated in Fig. 9, where we show T plotted against the normalized time $A\tau$ for medium density $\rho = 0.087$, $\rho = 0.9$ and different values of r , as given in the legend.

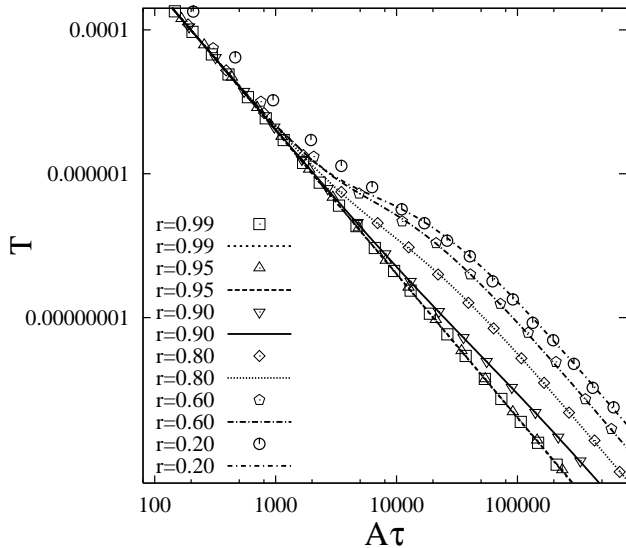


FIG. 9. T as function of rescaled time $A\tau$. The density is $\rho = 0.087$, $\rho = 0.9$ and the restitution coefficient r is given in the insert. The curves represent again the numerical solutions of Eqs. (21).

In the intermediate time regime all curves follow the

decay of smooth spheres [see Eq.(25)], which is independent of r , because we use scaled time $A\tau$. In the true asymptotic regime, all curves have the same slope with however an axial section, which increases with decreasing r . Without scaling with A the axial section decreases with decreasing r reflecting the more efficient dissipation of energy for smaller r . The agreement between theory and simulations is quite good for values of r as low as $r = 0.6$, and even for $r = 0.2$ only the crossover regime is not captured by theory.

V. SUMMARY AND DISCUSSION

Homogeneous cooling of colliding inelastic rough spheres has been investigated with numerical simulations and an approximate kinetic theory in two and three dimensions as well. We have confirmed that surface roughness is an important characteristic of the grains, in so far as it determines the decay of translational energy, i.e. the rate of cooling. If energy loss due to small normal and tangential restitution are comparable, then one observes an initial linear change of translational and rotational energy, followed by a crossover to the asymptotic regime, where both functions decay like t^{-2} . This regime is characterized by a constant ratio $T=R$, whose value depends on both, r and ρ . The dependence on ρ is nonmonotonic, the ratio being smallest for $\rho = 1$. This nonmonotonic dependence on ρ also holds for the crossover time, which is longest for $\rho = 1$. If the coefficients of normal and tangential restitution are such that energy is lost mainly due to normal restitution, then we observe an intermediate time regime, in between the initial linear change and the true asymptotic behaviour with constant ratio $T=R$. This intermediate regime is also characterized by an algebraic decay of translational and rotational energy: Translational energy decays like for smooth spheres (t^{-2}), whereas rotational energy decays with an exponent that depends continuously on r and ρ .

The theoretical approach is based on the assumption of a generalised homogeneous cooling state: The N -particle distribution is assumed to depend on time only via the average energies of translation and rotation. Based on this assumption we computed the time decay of translational energy and rotational energy without further approximations. Good agreement with numerical simulations was found for a large range of timescales and parameter sets, provided no density instability builds up. The initial linear change, the asymptotic t^{-2} behaviour, the crossover in between as well as the intermediate algebraic decay for almost smooth spheres - all these features are accurately reproduced by our theoretical ansatz. These findings certainly support the assumption of a homogeneous cooling state and suggest to expand around the HCS state to study deviations from homogeneous cooling.

ACKNOWLEDGEMENTS

S.L. thanks the SFB 382 (A 6), and M.H. thanks the Land Niedersachsen for financial support. S.M. gratefully acknowledges the support of the Alexander von Humboldt-Stiftung.

APPENDIX A: DETAILED CALCULATION IN 2D

In this appendix we explain, as an example, the main steps to calculate $iL_+^0 E_{tr, HCS}$ of Eq. (13) in 2D. The expectation value is calculated with the N -particle distribution function, properly normalised

$$H_{CS}(\{t\}) = \frac{1}{V^N} \prod_{i=1}^N \frac{m}{2T_{tr}(t)} \prod_{j=1}^N \frac{I}{2T_{rot}(t)} \exp \left[-\sum_{i=1}^N \frac{m}{2T_{tr}(t)} v_i^2 - \sum_{j=1}^N \frac{I}{2T_{rot}(t)} \dot{\phi}_j^2 \right] \quad (A1)$$

The angular velocity is a scalar in two dimensions, but a vector in more than two dimensions. Free streaming does not change the energy, so we have to take into account only the collision operator iL_+^0 and we keep the abbreviation for C_+ from Eq. (9) so that

$$iL_+^0 E_{tr, HCS} = \frac{1}{2N} \int \prod_{i=1}^N d\mathbf{r}_i \prod_{j=1}^N d\mathbf{r}_j \prod_{k=1}^N d\mathbf{r}_k \frac{1}{2N} \sum_{i=1}^N m v_i^2 = \frac{1}{2N} \int \prod_{i=1}^N d\mathbf{r}_i \prod_{j=1}^N d\mathbf{r}_j \prod_{k=1}^N d\mathbf{r}_k \frac{m}{2} v^2 + v'^2 \quad (A2)$$

The binary collision operator C_+ gives a contribution only, if either $\mathbf{r}_1 = \mathbf{r}_2$ or if $\mathbf{r}_1 = \mathbf{r}_2$. Next, we introduce two δ -functions,

$$iL_+^0 E_{tr, HCS} = \int \prod_{i=1}^N d\mathbf{r}_i \prod_{j=1}^N d\mathbf{r}_j \prod_{k=1}^N d\mathbf{r}_k \frac{1}{2N} \sum_{i=1}^N m v_i^2 + v'^2 ; \quad (A3)$$

which allows us to replace \mathbf{r}_1 by \mathbf{R}_1 and \mathbf{r}_2 by \mathbf{R}_2 in C_+ (9). Integration over all \mathbf{r}_i of the respective part of Eq. (A3) can then be performed and yields a factor

$$\int \prod_{i=1}^N d\mathbf{r}_i \prod_{j=1}^N d\mathbf{r}_j \prod_{k=1}^N d\mathbf{r}_k \frac{1}{2N} \sum_{i=1}^N m v_i^2 + v'^2 = V^N g(\mathbf{R}_{12}) \quad (A4)$$

The pair correlation function $g(\mathbf{R}_{12})$ depends on $\mathbf{R}_{12} = \mathbf{R}_1 - \mathbf{R}_2$ only. Similarly integration over all velocities

and angular velocities with index i and j gives 1 due to normalization. We can sum over $N(N-1)$ identical integrals and get

$$iL_+^0 E_{tr, HCS} = \frac{(N-1)}{2V^2} \frac{m}{2T_{tr}(t)} \int \prod_{i=1}^N d\mathbf{r}_i \prod_{j=1}^N d\mathbf{r}_j \prod_{k=1}^N d\mathbf{r}_k \frac{I}{2T_{rot}(t)} \exp \left[-\sum_{i=1}^N \frac{m}{2T_{tr}(t)} v_i^2 - \sum_{j=1}^N \frac{I}{2T_{rot}(t)} \dot{\phi}_j^2 \right] g(\mathbf{r}_{12} - \hat{\mathbf{r}}) \cdot (\mathbf{v}_{12} - \hat{\mathbf{r}}) \cdot (\mathbf{v}_{12} - \hat{\mathbf{r}}) \quad (A5)$$

The loss of translational energy of two colliding particles is denoted by E_{tr} and given by

$$E_{tr} = \frac{m}{2} \left[(1 - \dot{\phi}^2) (v_{12} - \hat{\mathbf{r}})^2 - (1 - \dot{\phi}'^2) (v_{12} - \hat{\mathbf{r}})^2 + 2 \dot{\phi}^2 a^2 \right] \quad (A6)$$

Here we use the abbreviations $\dot{\phi} = \frac{q(1+\dot{\phi})}{2q+2}$, $\dot{\phi}' = (\dot{\phi}_1 + \dot{\phi}_2) = \frac{p}{2}$, and $\mathbf{R}_1 - \mathbf{R}_2 = \mathbf{r} = r\hat{\mathbf{r}}$. To perform the remaining integrations we substitute

$$\dot{\phi} = \frac{1}{2} (\dot{\phi}_1 + \dot{\phi}_2); \quad \dot{\phi}' = \frac{1}{2} (\dot{\phi}_1 - \dot{\phi}_2); \quad (A7)$$

$$\mathbf{V} = \frac{1}{2} (\mathbf{v}_1 + \mathbf{v}_2); \quad \mathbf{v} = \frac{1}{2} (\mathbf{v}_1 - \mathbf{v}_2); \quad (A8)$$

$$\mathbf{r} = \mathbf{R}_1 - \mathbf{R}_2; \quad R = R_1; \quad (A9)$$

The Jacobian determinant for the above transformation is 1. Integration over $\dot{\phi}$, \mathbf{V} and R can be done, which all give the value 1 due to normalisation. The resulting integral is

$$iL_+^0 E_{tr, HCS} = \frac{(N-1)m}{4T_{tr}(t)V} \frac{2I}{2T_{rot}(t)} \int \prod_{i=1}^N d\mathbf{r}_i \prod_{j=1}^N d\mathbf{r}_j \prod_{k=1}^N d\mathbf{r}_k \exp \left[-\sum_{i=1}^N \frac{m}{2T_{tr}(t)} v_i^2 - \sum_{j=1}^N \frac{I}{2T_{rot}(t)} \dot{\phi}_j^2 \right] g(\mathbf{r} - \hat{\mathbf{r}}) \cdot (\mathbf{v} - \hat{\mathbf{r}}) \cdot (\mathbf{v} - \hat{\mathbf{r}}) \quad (A10)$$

The integration over \mathbf{r} yields $2ag(2a)$. Choosing e.g. $\hat{\mathbf{r}}$ to point along the x -axis, the integrals over linear and angular velocities can easily be done as moments of a Gaussian distribution. The result is independent of $\hat{\mathbf{r}}$, so that the integration over $\hat{\mathbf{r}}$ gives 2 . Finally we assume that $1/N$, approximate $N(N-1)$ and obtain the result of Eq. (13)

APPENDIX B: ED ALGORITHM

Simple ED algorithms update the whole system after each event, a method which is straightforward, but inefficient for large numbers of particles. In Ref. [20] an ED

algorithm was introduced which updates only those two particles which were involved in the last collision. For this a double buffering data structure is implemented, which contains the 'old' status and the 'new' status, each consisting of: time of event, position, velocities, and event-partner. When a collision occurs, the 'old' and 'new' status of the participating particles are exchanged. Thus, the former 'new' status becomes the actual 'old' one, while the former 'old' status becomes the 'new' one and is free for future calculations. This seemingly complicated exchange of information is carried out extremely simple and fast by only exchanging the pointers to the 'new' and 'old' status respectively. The 'old' status of particle i has to be kept in memory, in order to calculate the time of the next contact, t_{ij} , of particle i with any other object j which can change its status due to a collision with yet another particle. During the simulation this may be necessary several times so that the predicted 'new' status has to be modified. An object j is either a particle ($j = 1, \dots, i-1, i+1, \dots, N$) or a cell-wall ($j = N+1, \dots$). The minimum of all t_{ij} is stored in the 'new' status of particle i , together with the corresponding partner j . Depending on the implementation, also positions and velocities after the collision can be calculated. This would be a waste of computer time, since before the time t_{ij} , the predicted partners i and j might be involved into several collisions with other particles, so that we apply a delayed update scheme [20]. The minimum times of event, i.e. the times which indicate the next event for a certain particle, are stored in an ordered heap tree, such that the next event is found at the top of the heap with computational effort of $O(1)$; changing the position of one particle in the tree from the top to a new position needs $O(\log N)$ operations. The search for possible collision partners is accelerated by the use of a standard linked-cell data structure and consumes $O(1)$ of numerical resources. In total, this results in numerical effort of $O(N \log N)$ for N particles. For a detailed description of the algorithm see Ref. [20]. Using all these algorithmic tricks, we are able to simulate up to 10^5 particles within reasonable time on a small workstation (IBM P43/133M Hz) [21]. The particle number is limited by RAM-size (64M B) rather than CPU-power.

- [5] C. K. K. Lun and S. B. Savage, *J. Appl. Mech.* 54, 47 (1987).
- [6] C. K. K. Lun, *J. Fluid Mech.* 233, 539 (1991).
- [7] A. G. G. Oldshtein and M. Shapiro, *J. Fluid Mech.* 282, 75 (1995).
- [8] M. Huthmann and A. Zippelius, *Phys. Rev. E* 56, R6275 (1997).
- [9] S. Luding, *Phys. Rev. E* 52, 4442 (1995).
- [10] S. M. cNamara and S. Luding, (unpublished).
- [11] G. H. Bryan, *Brit. Assoc. Reports*, 83 (1894).
- [12] S. Chapman and T. G. Cowling, *The Mathematical Theory of Nonuniform Gases*, Cambridge University Press, London (1960).
- [13] M. H. E. Mst, J. R. Dorfmann, W. R. Hoegy, and J. M. J. van Leeuwen, *Physica* 45, 127 (1969).
- [14] T. P. C. van Noije, M. H. E. Mst, cond-mat/9706020 (unpublished).
- [15] R. Mazighi, B. Bemu, and F. Delyon, *Phys. Rev. E* 50, 4551 (1994).
- [16] S. M. cNamara and W. R. Young, *Phys. Rev. E* 50, R28 (1994).
- [17] S. Luding, E. Clement, J. Rajchenbach, and J. Duran, *Europhys. Lett.* 36, 247 (1996).
- [18] S. Luding, in *Powders & Grains 97* (Balkema, Amsterdam, 1997).
- [19] L. Verlet, *D. Levesque*, *Mol. Phys.* 46, 969 (1982)
- [20] B. D. Lubachevsky, *J. of Comp. Phys.* 94, 255 (1991).
- [21] S. Luding, M. Muller, and S. M. cNamara, in *Proceedings of the World Congress on Particle Technology* (Brighton, 1998), to appear.
- [22] S. M. cNamara, *Phys. Fluids A* 5, 3056 (1993).
- [23] J. P. Hansen and I. R. McDonald, *Theory of simple liquids*, Academic Press, London, 1990.

-
- [1] H. J. Herrmann, J.-P. Hovi, and S. Luding, eds., *Physics of dry granular media*, Kluwer Academic Publishers, Dordrecht, Netherlands, 1998.
 - [2] I. Goldhirsch and G. Zanetti, *Phys. Rev. Lett.* 70, 1619 (1993).
 - [3] S. M. cNamara and W. R. Young, *Phys. Rev. E* 53, 5089 (1996).
 - [4] J. T. Jenkins and M. W. Richmond, *Phys. of Fluids* 28, 3485 (1985).